PERGAMON

Computers and Structures 70 (1999) 635–646

Computers & Structures

A layer-wise triangle for analysis of laminated composite plates and shells

Salvador Botello [a], Eugenio Oñate [b], Juan Miquel Canet [b]

[a] *Facultad de Ingeniería Civil, Universidad de Guanajuato, Av. Juárez 77, 36000, Guanajuato, Gto., Mexico*
[b] *E.T.S. Ingenieros de Caminos, Canales y Puertos, Universidad Politécnica de Cataluña, Gran Capitáan s/n, 08034 Barcelona, Spain*

Received 20 January 1997; accepted 4 August 1998

Abstract

The paper presents a new triangle for analysis of laminate plates and shells. The in-plane degrees of freedom are interpolated quadratically whereas a linear layer-wise approximation is chosen for the normal displacement. A substructuring technique is used to eliminate the in-plane degrees of freedom during the assembly process thus reducing substantially the computationed costs. The element performance is evaluated in the static and dynamic analysis of different laminate plate and shell structures.

Keywords: Layer-wise triangle; Laminate plates; Static analysis; Dynamic analysis

1. Introduction

Layer-wise theory of composite plates was first developed by Reddy [1–3]. In this theory the three-dimensional displacement field is written as a linear combination of some function of the thickness coordinate and independent functions of the position within every layer as

$$u_i(x, y, z) - u_i^0(x, y) + \sum_{j=1}^{n_i} u_i^j(x, y)\Phi_j(z) \tag{1}$$

where n_i is the number of analysis layers taken across the thickness of the laminate and Φ_j are some known functions of the thickness coordinate z. The Φ_j functions are piecewise and continuous within every layer. They are only defined over two adjacent layers and it is possible to interpret them as global Lagrange interpolation functions associated with the common surface j (interface). Due to the local definition of Φ_j, the displacements are continuous across the thickness, but not their derivatives with respect to z. This implies that the shear strains are discontinuous at the interfaces, and consequently the shear stresses can be continuous for the case of layers with different mechanical properties, which is in agreement with experimental practice.

In this work a new triangular element with layer-wise approximation for the finite element analysis of composite plate and shell structures is presented. The element can be considered an extension of the linear/quadratic Reissner–Mindlin plate element based in an assumed shear strain approach formulated by Zienkiewicz et al. [4], Taylor and Papadopoulus [5] and Oñate et al. [6–8]. The inplane element displacements are interpolated linearly inside every layer and they are eliminated during the global assembly by means of a condensation technique. In the following sections details of the element formulation are presented, together with some examples of applications to static, dynamic and instability analysis of laminated composite plates and shells.

2. Triangular multilaminate plate element

Fig. 1 shows the geometry of the element. It is worth noting that the laminate is discretized into n analysis layers and $n + 1$ interfaces. The analysis layers can or cannot coincide with the real material layers. The horizontal displacements (in plane displacements) for the kth layer are interpolated as

0045-7949/99/$ - see front matter
PII: S0045-7949(98)00165-5

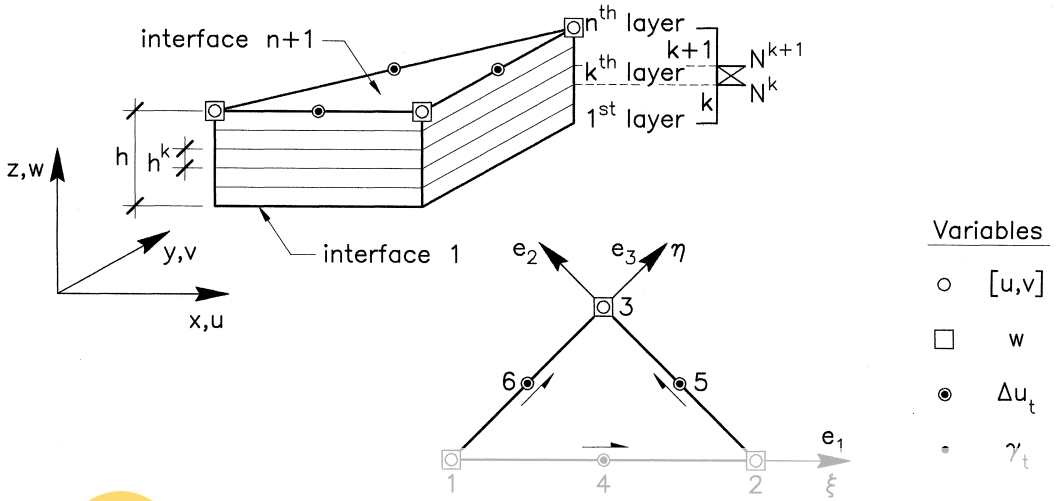

Fig. 1. Triangular plate element with layer-wise approximation.

$$\begin{Bmatrix} u \\ v \end{Bmatrix} = \sum_{i=1}^{3} N_i(\xi,\eta)\left[N^k(\zeta)\begin{Bmatrix} u_i^k \\ v_i^k \end{Bmatrix} + N^{k+1}(\zeta)\begin{Bmatrix} u_i^{k+1} \\ v_i^{k+1} \end{Bmatrix}\right] + \sum_{i=4}^{6} N_i(\xi,\eta)\mathbf{e}_{i-3}\left[N^k(\zeta)\Delta u_{t_i}^k + N^{k+1}(\zeta)\Delta u_{t_i}^{k+1}\right] \tag{2}$$

where $\Delta u_{t_i}^k$ $(i = 4, 5, 6)$ are the nodal displacement increments at the element mid-sides for the kth interface in the direction of the unit vectors $\mathbf{e}_{i-3}$ (Fig. 1). The normal displacement is assumed to be constant across the thickness and it is interpolated in terms of the corner values in the standard fashion as

$$w = \sum_{i=1}^{3} N_i(\xi,\eta) w_i \tag{3}$$

In Eqs. (2) and (3)

$$\begin{aligned} &N_i(\xi,\eta) = L_i \qquad i = 1,2,3 \\ &N_4(\xi,\eta) = 4L_1L_2, \quad N_5(\xi,\eta) = 4L_2L_3, \\ &N_6(\xi,\eta) = 4L_1L_3 \end{aligned} \tag{4}$$

where L_i are the linear shape functions for the three node triangle [9] and

$$N^k(\zeta) = \frac{1-\zeta}{2}, \quad N^{k+1}(\zeta) = \frac{1+\zeta}{2} \tag{5}$$

Eqs. (2) and (3) imply a hierarchical quadratic interpolation for the in-plane displacements u and v in the plane of every layer and a linear interpolation for w. Notice that for the case of a single analysis layer the element coincides with the linear/quadratic triangle developed in [4, 8].

The locking effect (which is usual in the Reissner–Mindlin plate formulation [20]) can be avoided by prescribing a transverse shear deformation field compatible with the assumed displacement field [6–8]. It is then necessary than the displacement, rotation and shear strain fields satisfy some compatibility conditions [4–9]. The shear strain field imposed in the present work is linear within the element giving a constant tangential shear strain along every element side [7, 20].

Eqs. (2)–(3) together with the imposed linear shear deformation field allow us to write for every layer the generalized bending and transverse shear deformations as

$$\boldsymbol{\varepsilon}_b = \mathbf{B}_b\mathbf{a}^k \quad \text{and} \quad \boldsymbol{\varepsilon}_s = \mathbf{B}_s\mathbf{a}^k \tag{6}$$

where

$$\boldsymbol{\varepsilon}_b = \left[\frac{\partial u}{\partial x}, \frac{\partial v}{\partial y}, \left(\frac{\partial u}{\partial y} + \frac{\partial v}{\partial x}\right)\right]^T; \qquad \boldsymbol{\varepsilon}_s = \left[\frac{\partial w}{\partial x} + \frac{\partial u}{\partial z}, \frac{\partial w}{\partial y} + \frac{\partial v}{\partial z}\right]^T \tag{7}$$

In the former expressions it has not been taken into account the normal shear strain ε_z following the usual hypothesis of plate theory ($\sigma_z = 0$). In Eq. (6) $\mathbf{B}_b$ and $\mathbf{B}_s$ are the bending and shear strain matrices for every layer detailed in Appendices A and B [10, 12] and $\mathbf{a}^k$ is the displacement vector for the kth layer given by

$$\mathbf{a}^{(k)} = \begin{Bmatrix} \mathbf{a}^k \\ \mathbf{a}^{k+1} \\ w_1 \\ w_2 \\ w_3 \end{Bmatrix} \tag{8}$$

where index k accounts for the variables in the kth interface and

$$\mathbf{a}^k = \left[u_1^k, v_1^k, u_1^k, v_2^k, u_3^k, v_3^k, \Delta u_{t_4}^k, \Delta u_{t_5}^k, \Delta u_{t_6}^k\right]^{\mathrm{T}} \tag{9}$$

The stiffness matrix for each layer is given by

$$\mathbf{K}^{(e)} = \int\int_{A^{(e)}} \int_{h^k} \mathbf{B}^{\mathrm{T}}\mathbf{D}\mathbf{B}\,\mathrm{d}V \tag{10}$$

where $\mathbf{B} = \begin{Bmatrix}\mathbf{B}_b \\ \mathbf{B}_s\end{Bmatrix}$ and $\mathbf{D}$ is the constitutive matrix for orthotropic plates [1–3, 20]. In Eq. (10) h^k and $A^{(e)}$ are the thickness and the interface area of the kth layer, respectively.

It is worth noting that the direction of the tangential shear needs to be uniquely defined for every element side shared by two elements. The signs in the $\mathbf{B}_w$ matrix of Appendix B correspond to the definition of the unit vectors $\mathbf{e}_i$ running from node k to node l, where $k < l$.

The volume integral Eq. (10) is performed for all layers. Due to the simplicity of the linear shape functions N^k it is possible to perform an explicit integration over the layer thickness h^k. A three Gauss point quadrature over the interface area $A^{(e)}$ is used.

3. Substructuring technique

The stiffness matrix assembly over the thickness follows the general rules for one-dimensional elements. This allows to eliminate the degrees of freedom in every layer $\mathbf{a}^k$ once the global stiffness matrix is obtained.

From Appendix C it follows immediately:

$$\mathbf{a}^k = \left[\mathbf{K}_{kk}^{(l)}\right]^{-1}\left[\mathbf{f}_k^{(l)} - \mathbf{K}_{k,k+1}^{(l)}\mathbf{a}^{k+1} - \mathbf{K}_{kw}^{(l)}\mathbf{a}_w\right] \tag{11}$$

The new equations system is now only written in terms of $\mathbf{a}^2, \mathbf{a}^3, \ldots, \mathbf{a}_w$.

Again it is possible to eliminate $\mathbf{a}^2$ (which corresponds to the second interface variables) in a similar way. This procedure is repeated for every layer, so that for the kth layer the displacements $\mathbf{a}^k$ are written as a function of the displacements corresponding to the $k+1$th layer, $\mathbf{a}^{k+1}$, and the vertical displacements $\mathbf{a}_w$.

This technique leads to a final condensed equations system which contains only the top layer displacements $\mathbf{a}^{n+1}$ and the vertical displacements $\mathbf{a}_w$. That is

$$\begin{bmatrix}\bar{\mathbf{K}}_{11} & \bar{\mathbf{K}}_{12} \\ \bar{\mathbf{K}}_{21} & \bar{\mathbf{K}}_{22}\end{bmatrix}\begin{Bmatrix}\mathbf{a}^{n+1} \\ \mathbf{a}_w\end{Bmatrix} = \begin{Bmatrix}\bar{\mathbf{f}}^{n+1} \\ \mathbf{f}_w\end{Bmatrix} \tag{12}$$

where $\bar{(\cdot)}$ are the modified stiffness matrices and nodal forces vectors. By solving Eq. (12) it is possible to obtain the displacements in the last interface $\mathbf{a}^{n+1}$ as well as the vertical displacements $\mathbf{a}_w$. Eq. (11) gives subsequently the displacements in every interface. This technique was initially suggested by Owen and Li [13–15] and it was later exploited by the authors of the present work [10–12].

4. Free vibration analysis

As the dominating modal shapes are vertically oriented and the vertical displacements are common for all laminates, the mass associated to the deflection w can be assigned to the last interface only ($\mathbf{M}_w$). Using again the same condensation technique previously explained, it is possible to obtain the stiffness matrix $\hat{\mathbf{K}}_w$ associated with the vertical displacements [12, 13, 16]. In this way the resulting simplified eigenproblem becomes

$$\left[\hat{\mathbf{K}}_w - \lambda^2\mathbf{M}_w\right]\mathbf{a}_w = \mathbf{0} \tag{13}$$

Eq. (13) is solved using standard techniques to obtain the eigenfrequencies λ. The eigenvectors containing the horizontal laminate displacements can be obtained by back-substituting in the expressions of the condensation process.

5. Non linear analysis

The effect of non linear large displacements can be easily included. In this work Von-Karman's assumptions have been used together with a total lagrangian formulation. The non-linear equation system is solved by a Newton–Raphson procedure. The same condensation technique is used to obtain the incremental displacements for every iteration. In this case $\mathbf{K}$ is the tangent stiffness matrix and $\mathbf{f}$ is the residual force vector. Note that only the displacements corresponding to the last laminate are involved in the condensed solution of the iterative system. It is however necessary to compute the whole residual force vector in order to check convergence [12].

6. Initial stability analysis

The initial stability problem is solved following standard eigenvalue procedures [9]. It is also possible in this case to use the condensation technique as explained for the case of free vibration analysis (viz Eq. (13)), thus reducing the total number of degrees of freedom in the eingenproblem [12].

7. Dynamic analysis

The condensation technique is used again to write the dynamic equations only in terms of the vertical

displacements, i.e.

$$\bar{\mathbf{M}}\ddot{\mathbf{a}}_w + \bar{\mathbf{C}}\dot{\mathbf{a}}_w + \bar{\mathbf{K}}\mathbf{a}_w = \mathbf{f}_w(t) \tag{14}$$

where $(\bar{\cdot})$ refers to the matrices associated with the vertical displacements (after condensing the in-plane nodal variables). In this work the damping matrix is taken as a linear function of the mass and stiffness matrices, that is

$$\bar{\mathbf{C}} = \alpha_0 \bar{\mathbf{M}} + \alpha_1 \bar{\mathbf{K}} \tag{15}$$

where the parameters α_0 and α_1 are calculated from two given damping ratios corresponding to two decoupled equations [12]. The time integration of Eq. (14) has been performed in this work using the standard Newmark algorithm [9].

8. Extension to laminated shell analysis

The previous plate triangle can be extended to the case of laminated shells. First it is necessary to consider first the kinematics of the element, which is defined with respect to a local cartesian axes system x', y', z'. The local axes x' and y' define the directions of the inplane displacements u', v', whereas z' defines the normal displacement w'. Once the stiffness matrix is obtained in this local system, it is transformed to global axes (Fig. 2) in the usual way.

As in the plate's case it is possible to define n analysis layers and $n+1$ interfaces. The displacements u', v' in the element plane corresponding to the kth layer are interpolated by [1–3]:

$$\begin{Bmatrix} u' \\ v' \end{Bmatrix} = \sum_{i=1}^{3} N_i(\xi,\eta) \left[\begin{Bmatrix} u'_{oi} \\ v'_{oi} \end{Bmatrix} + N^k(\zeta) \begin{Bmatrix} u_i'^k \\ v_i'^k \end{Bmatrix} + N^{k+1}(\zeta) \begin{Bmatrix} u_i'^{k+1} \\ v_i'^{k+1} \end{Bmatrix} \right] + \sum_{i=4}^{6} N_i(\xi,\eta)\, \mathbf{e}_{i-3} \left[N^k(\zeta) \Delta u_{t_i}^k + N^{k+1}(\zeta) \Delta u_{t_i}^{k+1} \right] \tag{16}$$

where $\begin{Bmatrix} u'_{oi} \\ v'_{oi} \end{Bmatrix}$ are constant (rigid-body) in-plane displacements across the thickness of the laminate, $\begin{Bmatrix} u_i'^k \\ v_i'^k \end{Bmatrix}$ are the in-plane displacements which are variable over the thickness and $\Delta u_{t_i}^k$ are the in-plane displacement increments in the midside nodes of the triangle in the directions defined by the tangent vectors $\mathbf{e}_{i-3}$ (Fig. 1).

The normal displacement w' is assumed to be constant throughout the thickness. Following this hypothesis it is possible to write

$$w' = \sum_{i=1}^{3} N_i(\xi,\eta) w'_i \tag{17}$$

In Eqs. (16) and (17) the shape functions are the same that those given by Eqs. (4) and (5).

Eqs. (16) and (17) define a quadratic interpolation over every interface for the in-plane displacements u' and v' and a linear interpolation for the displacement w'.

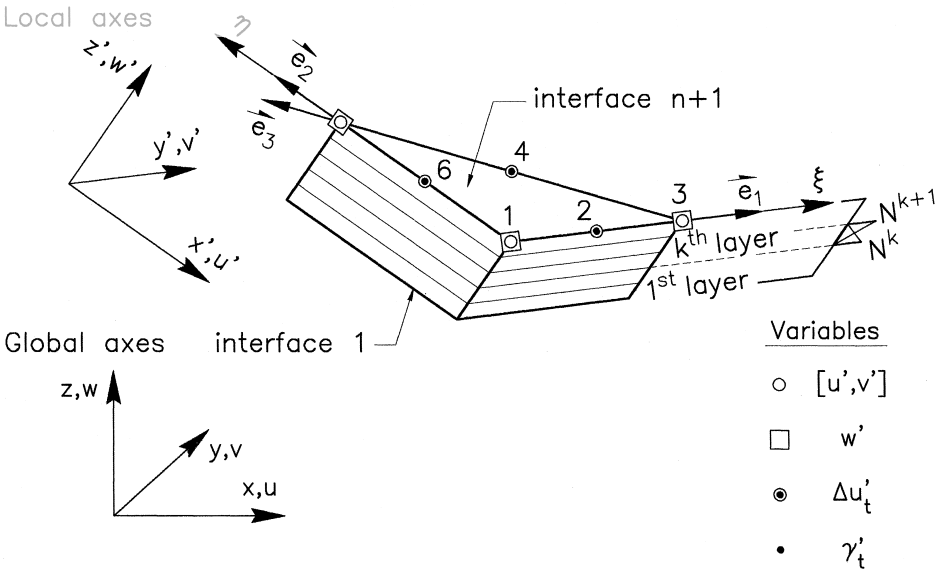

Fig. 2. Plane shell composite triangle.

The local strains for the kth layer are written

$$\boldsymbol{\varepsilon}'_{\mathrm{b}} = \left[\frac{\partial u'}{\partial x'}, \frac{\partial v'}{\partial y'}, \left(\frac{\partial u'}{\partial y'} + \frac{\partial v'}{\partial x'}\right)\right]^{\mathrm{T}} = \mathbf{B}_{\mathrm{b}} a' \tag{18}$$

$$\boldsymbol{\varepsilon}'_{\mathrm{s}} = \left[\left(\frac{\partial w'}{\partial x'} + \frac{\partial u'}{\partial z'}\right), \left(\frac{\partial w'}{\partial y'} + \frac{\partial v'}{\partial z'}\right)\right]^{\mathrm{T}} = \mathbf{B}_{\mathrm{s}} a' \tag{19}$$

where $\boldsymbol{\varepsilon}'_{\mathrm{b}}$ are the local strains accounting for membrane and bending effects and $\boldsymbol{\varepsilon}'_{\mathrm{s}}$ are the transverse shear strains. See Appendix D for a more detailed definition of $\mathbf{B}_{\mathrm{b}}$ and $\mathbf{B}_{\mathrm{s}}$ matrices.

The local displacement vector $\mathbf{a}'$ is written for the kth layer as

$$\mathbf{a}' = \begin{Bmatrix} \mathbf{a}'^{k} \\ \mathbf{a}'^{k+1} \\ \mathbf{a}'_0 \end{Bmatrix} \tag{20}$$

where

$$\mathbf{a}'^{k} = \left[u'^{k}_1, v'^{k}_1, w'^{k}_1, u'^{k}_2, v'^{k}_2, w'^{k}_2, u'^{k}_3, v'^{k}_3, w'^{k}_3, \Delta u'^{k}_{t4}, \Delta u'^{k}_{t5}, \Delta u'^{k}_{t6}\right]^{\mathrm{T}}$$

$$\mathbf{a}'_0 = \left[u'_{01}, v'_{01}, w'_{01}, u'_{02}, v'_{02}, w'_{02}, u'_{03}, v'_{03}, w'_{03}\right]^{\mathrm{T}} \tag{21}$$

In $\mathbf{a}'_0$ the normal displacement w'_{oi} has been introduced to simplify the transformation process although its contribution to the local strain matrices is zero.

The local displacements $\mathbf{a}'$ are transformed to global axes by

$$\mathbf{a}' = \bar{\mathbf{T}}\mathbf{a} \tag{22a}$$

where

$$\mathbf{a} = \begin{Bmatrix} \mathbf{a}^{k} \\ \mathbf{a}^{k+1} \\ \mathbf{a}^{0} \end{Bmatrix} \tag{22b}$$

and

$$\mathbf{a}^{k} = \left[u^{k}_1, v^{k}_1, w^{k}_1, u^{k}_2, v^{k}_2, w^{k}_2, u^{k}_3, v^{k}_3, w^{k}_3, \Delta u^{k}_{t4}, \Delta u^{k}_{t5}, \Delta u^{k}_{t6}\right]^{\mathrm{T}}$$

$$\mathbf{a}_0 = \left[u_{01}, v_{01}, w_{01}, u_{02}, v_{02}, w_{02}, u_{03}, v_{03}, w_{03}\right]^{\mathrm{T}} \tag{22c}$$

where the transformation matrix is given by

$$\bar{\mathbf{T}} = \begin{bmatrix} \hat{\mathbf{T}} & \mathbf{0} & \mathbf{0} \\ \mathbf{0} & \mathbf{T} & \mathbf{0} \\ \mathbf{0} & \mathbf{0} & \mathbf{T}' \end{bmatrix} \quad \text{with} \quad \hat{\mathbf{T}} = \begin{bmatrix} \hat{\mathbf{T}}' & \mathbf{0} \\ \mathbf{0} & \mathbf{I}_3 \end{bmatrix} \tag{23}$$

where $\hat{\mathbf{T}}$ is the $\mathbf{I}_3$ identity 3×3 matrix and

$$\hat{\mathbf{T}}' = \begin{bmatrix} \mathbf{T} & & \mathbf{0} \\ & \mathbf{T} & \\ \mathbf{0} & & \mathbf{T} \end{bmatrix}, \quad \mathbf{T} = \begin{bmatrix} \lambda_{x'x} & \lambda_{x'y} & \lambda_{x'z} \\ \lambda_{y'x} & \lambda_{y'y} & \lambda_{y'z} \\ \lambda_{z'x} & \lambda_{z'y} & \lambda_{z'z} \end{bmatrix} \tag{24}$$

and $\lambda_{x'x}$ is the cosinus of the angle between axes x' and x etc. (Fig. 2).

The global stiffness matrix for the kth layer is obtained by the standard transformation

$$\mathbf{K}^{(e)} = \bar{\mathbf{T}}^{\mathrm{T}} \mathbf{K}'^{(e)} \bar{\mathbf{T}} \tag{25}$$

where the local stiffness matrix is given by

$$\mathbf{K}'^{(e)} = \int_{A^{(e)}} \mathbf{B}^{\mathrm{T}} \mathbf{D} \mathbf{B} \, \mathrm{d}V \tag{26}$$

where $\mathbf{B} = \begin{Bmatrix} \mathbf{B}_{\mathrm{b}} \\ \mathbf{B}_{\mathrm{s}} \end{Bmatrix}$ and $\mathbf{D}$ is the local constitutive matrix for orthotropic materials [1–3].

A more detailed version of the local stiffness matrix $\mathbf{K}'^{(e)}$ is given in Appendix E.

As in the case of multilaminated plates, it is necessary to define a unique direction for the transverse shear over the common side of two adjacent elements. The signs of $\mathbf{B}_{\mathrm{w}}$ in Appendix E, correspond again to the definition of the $\mathbf{e}_i$ vector running from node k to node l, with $k < l$ [5–12].

The integration across the thickness is performed explicitly, whereas the integration over the surface of every interface is made by means of a three-point Gauss quadrature.

Again it is possible to use the condensation technique across the thickness in order to reduce the number of calculations. The procedure consists now in eliminating the global displacements of the lower interlaminar surface $\mathbf{a}^k$ for every layer k as a function of $\mathbf{a}^{k+1}$ and $\mathbf{a}^0$ by means of an expression similar to Eq. (11). Further details can be found in [12].

9. Examples

9.1. Simply supported square laminated plate

The first example studied is a graphite–epoxy simply supported plate. The geometry and material properties are shown in Fig. 3. We consider five laminates with orientations $0°/90°/0°/90°/0°$ and thickness $\frac{h}{6}/\frac{h}{4}/\frac{h}{6}/\frac{h}{4}/\frac{h}{6}$. The distributed load over the plate is given by $q = q_0 \sin \pi x/a \sin \pi y/a$.

For symmetry reasons only a quarter of plate was analyzed. The discretization is shown in Fig. 3. The number of analysis layers was taken the same as the number of laminates. Table 1 shows some results for the vertical displacement at the center of the plate and the stresses in some characteristic points, for different side length/thickness ratios (a/h). In order to show the accuracy of the results, they are compared with the solution obtained by Stavsky [18] by means of the Classical Theory of Laminated Plates (CLPT) which is based on Kirchhoff's hypothesis. Note the difference of the results when the thickness increases. This discrepancy is due to the effect of shear deformation which is important for thick plates. Indeed this effect can not be reproduced with CLPT.

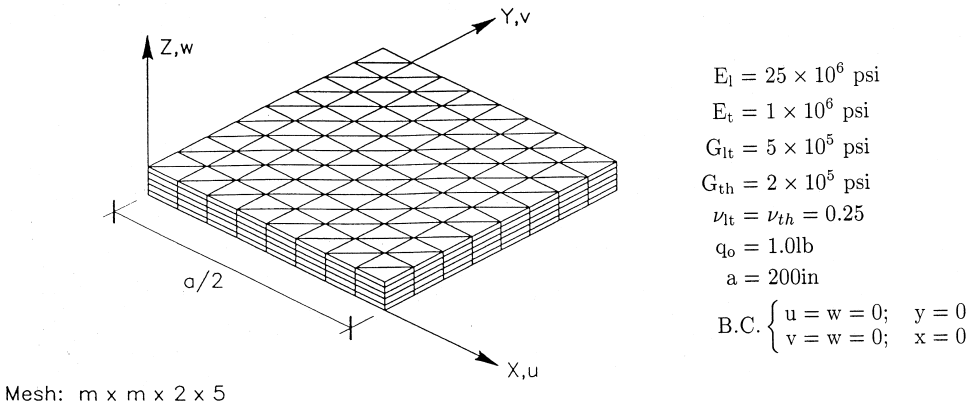

Fig. 3. Simply supported square laminated plate (five graphite-epoxy laminates) geometry and material properties.

It is worth mentioning the reduction of degrees of freedom by means of the condensation technique. In this case the reduction was from 1984 to 384 d.o.f. If the number of layers is further increased the total number or degrees of freedom after the condensation procedure will be the same plus the additional vertical degrees of freedom.

9.2. Free vibration analysis of a simply supported square laminated plate

The side length/thickness ratio in this case is $a/h = 10$ and the laminated sequence is 90°/0°/.../90°/0°. The thickness is the same for every laminate. The material properties are:

$$\frac{G_{lt}}{E_t} = 0.5; \quad \frac{G_{lh}}{E_t} = 0.2; \quad \nu_{lt} = \nu_{lh} = 0.25, \quad l = 1.0$$

The analysis was repeated for different E_l/E_t ratios (l = longitudinal direction, t = transversal direction, h = thickness direction). The mesh was regular containing $8 \times 8 \times 2 \times n$ elements, where n is the number of analysis layers. In all cases the number of layers (n) was taken equal to the number of laminates.

Table 2 displays the normalized results for the first vibration frequency.

Table 1
Vertical displacement and stresses in the center of a simply supported graphite–epoxy laminated plate (five laminates) under a sinusoidal distributed load. CLPT: results obtained with classical laminate plate theory [8]

MESH	i a/h	w_c (a/2, a/2)	$\bar{\sigma}_x$ (a/2, a/2, ±h/2)	$\bar{\sigma}_y$ (a/2, a/2, ±h/2)	$\bar{\tau}_{xz}$ (0, a/2, 0)	τ_{yz} (a/2, 0, 0)
$m = 2$	4	5.0097	±.585	±.397	.160	.171
$m = 4$	4	5.6431	±.625	±.455	.202	.212
$m = 8$	4	5.7582	±.625	±.473	.21775	.226
CLPT	4	4.291	±.651	±.626	N.A.	.233
$m = 2$	20	1.0226	±.4575	±.340	.170	.151
$m = 4$	20	1.1624	±.5225	±.373	.228	.191
$m = 8$	20	1.1946	±.535	±.378	.250	.207
CLPT	20	1.145	±.539	±.380	.268	.212
$m = 2$	100	.8439	±.468	±.318	.178	.148
$m = 4$	100	.971693	±.528	±.396	.259	.186
$m = 8$	100	1.001176	±.539	±.362	.272	.210
CLPT	100	1.0	±.539	±.359	.272	.205

$$w_c = \frac{\pi^4 Q w}{12 s^4 h q_0}$$

$$(\bar{\sigma}_x, \bar{\sigma}_y) = \frac{1}{q_0 s^2}(\sigma_x, \sigma_y)$$

$$(\bar{\tau}_x, \bar{\tau}_y) = \frac{1}{q_0 s^2}(\tau_x, \tau_y), \quad s = a/h$$

$$Q = 4G_{lt} + \left[E_l + E_t(1 + 2\nu_{th})\right]/(1 - \nu_{lt}\nu_{th})$$

Table 2
Normalized material frequencies for a simply supported laminated square plate ($a/h = 10$)

	No. of layers (n)	$E_l/E_t = 3$	$E_l/E_t = 10$	$E_l/E_t = 20$	$E_l/E_t = 30$	$E_l/E_t = 40$
Noor [17]	2	0.25031	0.27938	0.30698	0.32705	0.34250
CLPT	2	0.27082	0.30968	0.35422	0.39335	0.42884
This work	2	0.2623	0.29746	0.32758	0.34904	0.36550
Noor	4	0.26182	0.32578	0.37622	0.40660	0.42719
CLPT	4	0.28676	0.38877	0.49907	0.58900	0.66690
This work	4	0.2688	0.3364	0.38787	0.41846	0.43904
Noor	6	0.26440	0.33657	0.39359	0.42783	0.45091
CLPT	6	0.28966	0.40215	0.52234	0.61963	0.70359
This work	6	0.2702	0.3465	0.401163	0.43452	0.456819
Noor	10	0.26583	0.34350	0.40337	0.44011	0.46498
CLPT	10	0.29115	0.40888	0.53397	0.63489	0.72184
This work	10	0.2795	0.3492	0.40875	0.44397	0.467593

$$\hat{\lambda} = \frac{\lambda a^2}{h} / \frac{l}{E_t}.$$

The results obtained agree well with those reported by Noor [17] and also with those obtained using the classical laminate plate theory (CLPT).

9.3. Stability analysis of a simply supported laminated square plate

The same laminated plate of the previous example was analyzed with the following material properties:

$$\frac{G_{lt}}{E_t} = 0.6; \quad \frac{G_{lh}}{E_t} = 0.5; \quad \nu_{lt} = \nu_{lh} = 0.25$$

The mesh contained now $4 \times 4 \times 2 \times n$ elements. Again the number of layers was varied, with that of laminates. The plate was compressed symmetrically from two opposite sides.

Table 3 shows the normalized values for the critical load,

$$N_{cr} = \frac{\sigma_{cr} a^2}{E_t h^2},$$

for different E_l/E_t ratios. Results are compared with those obtained by other authors [13,17]. The discrepancy of the results obtained with CLPT grows as the ratio E_l/E_t increases. This shows the inability of CLP theory to model high E_l/E_t ratios as already shown by some authors [17].

9.4. Dynamic analysis of a simply supported laminate plate

This case studied a simply supported laminated plate with two laminates oriented as 0°/90°. Every laminate have the same thickness. The material proper-

Table 3
Normalized value of the critical load for a simply supported laminated plate ($a/h = 10$)

No. of layers (n)		E_l/E_t 3	10	20	30	40
3	Present work	5.2570	10.0860	15.6015	19.9915	23.5920
	Owen and Li [13]	5.4026	9.9590	15.3201	19.6872	23.3330
	Noor [17]	5.3044	9.7621	15.0191	19.3040	22.8807
	CLPT	5.7538	11.4920	19.7120	27.9360	36.1600
5	Present work	5.2545	10.2150	15.0890	20.9170	24.9695
	Owen and Li	5.4208	10.1609	15.9976	20.9518	25.2150
	Noor	5.3255	9.9603	15.6527	20.4663	24.5929
	CLPT	5.7538	11.4920	19.7120	27.9360	36.1600
9	Present work	5.2530	10.2800	16.3385	21.3980	25.9695
	Owen and Li	5.4187	10.1990	16.1560	21.2697	25.7093
	Noor	5.3352	10.0417	15.9153	20.9614	25.3436
	CLPT	5.7538	11.4920	19.7120	27.9360	36.1600

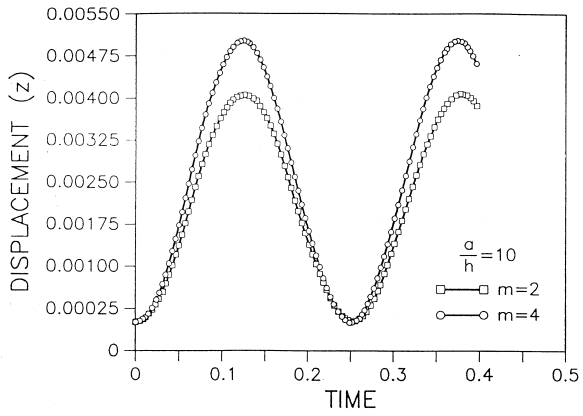

Fig. 4. Undamped time evolution of the vertical displacement in the center of a simply supported laminated plate ($a/h = 10$) with two laminates. Results are shown for two different meshes; $m = 2$ and $m = 4$.

ties are:

$$E_l = 25 \times 10^6 \text{ psi}, \quad E_t = 1 \times 10^6 \text{ psi}$$

$$G_{lt} = 5 \times 10^5 \text{ psi}, \quad G_{lh} = 2 \times 10^5 \text{ psi}$$

$$\nu_{lt} = \nu_{lh} = 0.3, \quad a = 100.0 \text{ in}$$

The boundary conditions are:

$$u = 0 \quad \text{and} \quad y = 0, \quad y = a/2,$$
$$v = 0 \quad \text{and} \quad x = 0, \quad x = a/2,$$
$$w = 0 \quad \text{and} \quad x = 0, \quad y = 0$$

The load is a heavyside function varying on time and with the following surface distribution:

$$q = q_0 \sin\frac{\pi x}{a} \sin\frac{\pi y}{a}; \qquad q_0 = 1.0$$

Fig. 4 shows the undamped time evolution of the vertical displacement in the center of the plate for the case of $a/h = 10$ and two layers. Again one-quarter of the plate was analyzed due to symmetry. Results are shown for two different meshes ($m = 2$ and $m = 4$) giving practically the same period and small changes in the amplitudes. The same results are practically obtained when the number of analysis layers increases.

9.5. Simply supported cylindrical laminated shell

This example corresponds to a simply supported laminated cylindrical shell. The shell is composed by three graphite-epoxy layers of high elastic modulus. The orientations are 90°/0°/90° referred to the global y-axis (Fig. 5). Fig. 5 also shows the geometry and material properties.

The analysis is made by considering three different meshes: 4 × 4, 6 × 6 and 8 × 8 elements. For computational purposes the thickness is divided into 3, 6 and 24 analysis layers for the 4 × 4 mesh and in 24

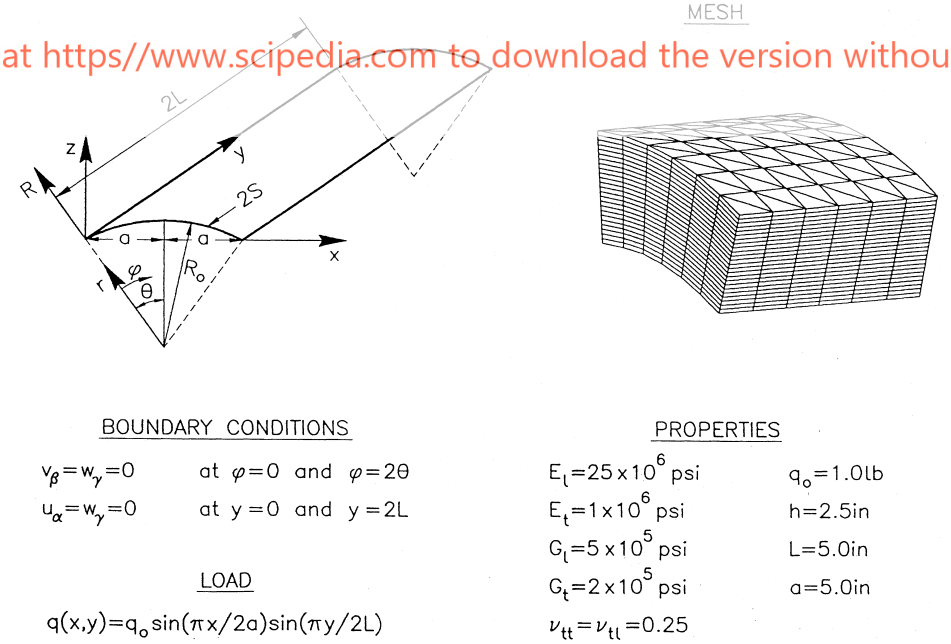

Fig. 5. Simply supported laminated shell (three graphite-epoxy layers with orientations 90°/0°/90° referred to the global y-axis). Geometry and material properties ($\theta = 30°$).

Table 4
Some displacements and stresses for the laminate cylindrical shell

Mesh	Analysis layers		*theta\rm* $=30^\circ$ *u* displ. point	value	*v* displ. point	value	σ_{xx} point	value	σ_{yy} point	value
4×4	3	Max	$(a, L/2, h)$	0.257×10^{-6}	$(a, 0, h)$	0.325×10^{-5}	$(a, L/2, 0)$	6.86	$(a, L/2, h/3)$	3.15
		Min	$(0, L/2, h)$	-0.457×10^{-5}	$(a, 0, 0)$	-0.282×10^{-5}	$(a, L/2, h)$	−7.67	$(a, L/2, 2h/3)$	−6.15
	6	Max	$(a, L/2, h)$	0.334×10^{-6}	$(a, 0, h)$	0.337×10^{-5}	$(a, L/2, 0)$	9.18	$(a, L/2, h/3)$	3.50
		Min	$(0, L/2, 0)$	-0.507×10^{-5}	$(a, 0, 0)$	-0.294×10^{-5}	$(a, L/2, h)$	−9.47	$(a, L/2, 2h/3)$	−6.56
	24	Max	$(a, L/2, h)$	0.379×10^{-6}	$(a, 0, h)$	0.346×10^{-5}	$(a, L/2, 0)$	10.90	$(a, L/2, h/3)$	3.90
		Min	$(0, L/2, 0)$	-0.525×10^{-5}	$(a, 0, 0)$	-0.303×10^{-5}	$(a, L/2, h)$	−10.60	$(a, L/2, 2h/3)$	−7.00
6×6	24	Max	$(a, L/2, h)$	0.374×10^{-6}	$(a, 0, h)$	0.358×10^{-5}	$(a, L/2, 0)$	10.70	$(a, L/2, h/3)$	3.94
		Min	$(0, L/2, 0)$	-0.535×10^{-5}	$(a, 0, 0)$	-0.312×10^{-5}	$(a, L/2, h)$	−10.30	$(a, L/2, 2h/3)$	−7.31
8×8	24	Max	$(a, L/2, h)$	0.373×10^{-6}	$(a, 0, h)$	0.361×10^{-5}	$(a, L/2, 0)$	10.80	$(a, L/2, h/3)$	4.00
		Min	$(0, L/2, 0)$	-0.539×10^{-5}	$(a, 0, 0)$	-0.317×10^{-5}	$(a, L/2, h)$	−10.20	$(a, L/2, 2h/3)$	−7.34

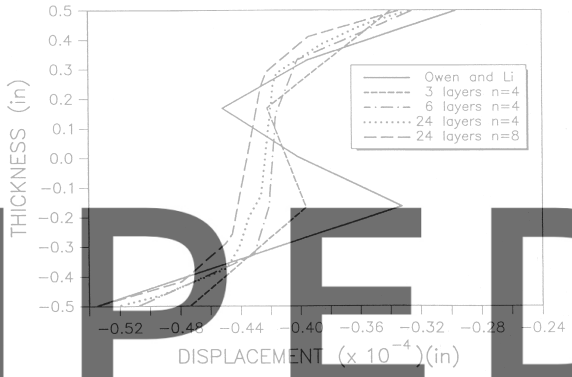

Fig. 6. Thickness variations of in-plane displacements for the laminate cylindrical shell ($x = 0$, $y = L$) for different meshes and layers.

layers for the other meshes. Table 4 shows some numerical results for the displacement and stresses at different points. The variation of the displacements across the thickness is shown in Fig. 6. Fig. 7 displays the distribution of σ_{yz} and σ_{xz} across the thickness.

The performance of the new element for small and high E_l/E_t ratios is quite good as compared with the work of other authors [13,17]. Again CLP theory shows a deficient performance for high E_l/E_t ratios.

10. Conclusions

The proposed triangular element combines the benefit from a layer-wise approximation and an assumed

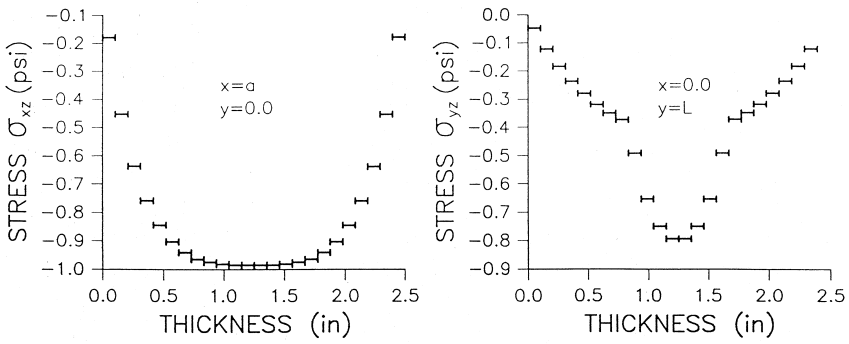

Fig. 7. Cylindrical shell. Thickness distribution of σ_{yz} and σ_{xz}.

shear strain model adequate for the analysis of thin and thick laminated plates and shells. The interpolation across the thickness allows a condensation to be performed for every layer, which reduces drastically the total number of degrees of freedom in the final system. The examples show the good behavior of the element for analysis of laminated composite plates and shells.

Appendix A

A.0.1. Bending strain matrix for the proposed plate triangle

$$\mathbf{B}_{\mathrm{b}} = \left[\mathbf{B}_{\mathrm{b}}^{k}, \mathbf{B}_{\mathrm{b}}^{k+1}, \mathbf{0}\right]$$

$$\mathbf{B}_{\mathrm{b}}^{k} = \left[\mathbf{B}_{\mathrm{b}_1}^{k}, \mathbf{B}_{\mathrm{b}_2}^{k}, \mathbf{B}_{\mathrm{b}_3}^{k}, \bar{\mathbf{B}}_{\mathrm{b}_4}^{k}, \bar{\mathbf{B}}_{\mathrm{b}_5}^{k}, \bar{\mathbf{B}}_{\mathrm{b}_6}^{k}\right]$$

with

$$\mathbf{B}_{\mathrm{b}_i}^{k} = \begin{bmatrix} \dfrac{\partial N_i}{\partial x} N^k & 0 \\ 0 & \dfrac{\partial N_i}{\partial y} N^k \\ \dfrac{\partial N_i}{\partial y} N^k & \dfrac{\partial N_i}{\partial x} N^k \end{bmatrix} \quad i = 1, 2, 3$$

$$\bar{\mathbf{B}}_{\mathrm{b}_i}^{k} = \mathbf{B}_{\mathrm{b}_{ij}}^{k} \mathbf{e}_i \otimes \mathbf{e}_i \quad i = 4, 5, 6$$

c_i, s_i = components of the unit vector $\mathbf{e}_i = [c_i,\ s_i]^{\mathrm{T}}$ $(i = 1,2,3)$

Appendix B

B.0.1. Shear deformation matrix for the proposed plate triangle

$$\mathbf{B}_{\mathrm{s}} = \mathbf{J}^{-1}\mathbf{M}\left[\mathbf{B}_{\mathrm{s}}^{k}, \mathbf{B}_{\mathrm{s}}^{k+1}, \mathbf{B}_{\mathrm{w}}\right]$$

$$\mathbf{B}_{\mathrm{s}}^{k} = \begin{bmatrix} a_{12} & b_{12} & a_{12} & b_{12} & 0 & 0 & c_{12} & 0 & 0 \\ 0 & 0 & \dfrac{a_{23}}{\sqrt{2}} & \dfrac{b_{23}}{\sqrt{2}} & \dfrac{a_{23}}{\sqrt{2}} & \dfrac{b_{23}}{\sqrt{2}} & 0 & \dfrac{c_{23}}{\sqrt{2}} & 0 \\ a_{31} & b_{31} & 0 & 0 & a_{32} & b_{32} & 0 & 0 & c_{32} \end{bmatrix}$$

$$\mathbf{B}_{\mathrm{s}}^{k+1} = -\mathbf{B}_{\mathrm{s}}^{k}$$

$$\mathbf{B}_{\mathrm{w}} = \begin{bmatrix} -1 & 1 & 0 \\ 0 & -1/\sqrt{2} & 1/\sqrt{2} \\ -1 & 0 & 1 \end{bmatrix},$$

$$\mathbf{M} = \begin{bmatrix} 1-\eta & -\sqrt{2}\eta & \eta \\ \xi & \sqrt{2}\xi & 1-\xi \end{bmatrix}$$

$$a_{ij} = -\frac{c_i l^{ij}}{2h^k}; \quad b_{ij} = -\frac{s_i l^{ij}}{2h^k}; \quad c_{ij} = -\frac{2l^{ij}}{3h^k}$$

c_i, s_i = unit vectors components $\mathbf{e}_i = [c_i,\ s_i]^{\mathrm{T}}$ $(i = 1,2,3)$

l^{ij} → length of the element side ij

h^k → thickness of the layer k

$\mathbf{J}$ = jacobian matrix $(\xi,\eta \to xy)$

Appendix C

C.0.1. General form of the global equations system for a laminate plate with n layers

$$\begin{bmatrix} \mathbf{K}_{11}^{(1)} & \mathbf{K}_{12}^{(2)} & \mathbf{0} & \mathbf{0} & \cdots & \mathbf{K}_{13}^{(1)} \\ \mathbf{K}_{21}^{(1)} & \left(\mathbf{K}_{22}^{(2)} + \mathbf{K}_{11}^{(2)}\right) & \mathbf{K}_{12}^{(2)} & \mathbf{0} & \cdots & \left(\mathbf{K}_{23}^{(1)} + \mathbf{K}_{13}^{(2)}\right) \\ \mathbf{0} & \mathbf{K}_{21}^{(2)} & \left(\mathbf{K}_{22}^{(2)} + \mathbf{K}_{11}^{(3)}\right) & \mathbf{K}_{12}^{(3)} & \cdots & \left(\mathbf{K}_{23}^{(2)} + \mathbf{K}_{13}^{(3)}\right) \\ & & & & \ddots & \vdots \\ & & & & \mathbf{K}_{22}^{(n)} & \mathbf{K}_{23}^{(n)} \\ & & & & & \mathbf{K}_{\mathrm{ww}}^{(n)} \end{bmatrix}$$

$$\begin{Bmatrix} \mathbf{a}^1 \\ \mathbf{a}^2 \\ \mathbf{a}^3 \\ \vdots \\ \vdots \\ \mathbf{a}^{n+1} \\ \mathbf{a}_{\mathrm{w}} \end{Bmatrix} = \begin{Bmatrix} \mathbf{f}^1 \\ \mathbf{f}^2 \\ \mathbf{f}^3 \\ \vdots \\ \vdots \\ \mathbf{f}^{n+1} \\ \mathbf{f}_{\mathrm{w}} \end{Bmatrix}$$

$\mathbf{K}^{(k)}{}_{ij}$ = stiffness matrix linking points i and j of the kth layer

$\mathbf{a}^k$ = in-plane nodal displacements for the kth interface

$\mathbf{a}_{\mathrm{w}} = [w_1,\ w_2, \ldots, w_n]^{\mathrm{T}}$

Appendix D

D.0.1. Local strain matrices for the triangular shell element

$$\underset{(3\times33)}{\mathbf{B}_{\mathrm{b}}} = \underset{(3\times12)}{\left[\mathbf{B}_{\mathrm{b}}^{k},\right.} \quad \underset{(3\times12)}{\mathbf{B}_{\mathrm{b}}^{k+1},} \quad \underset{(3\times9)}{\left.\mathbf{B}_{\mathrm{b}}^{o}\right]}$$

$$\mathbf{B}_{\mathrm{b}}^{k} = \left[\mathbf{B}_{\mathrm{b}_1}^{k}, \mathbf{B}_{\mathrm{b}_2}^{k}, \mathbf{B}_{\mathrm{b}_3}^{k}, \bar{\mathbf{B}}_{\mathrm{b}_4}^{k}, \bar{\mathbf{B}}_{\mathrm{b}_5}^{k}, \bar{\mathbf{B}}_{\mathrm{b}_6}^{k}\right]$$

with

$$\mathbf{B}_{\mathrm{b}_i}^{o} = \begin{bmatrix} \dfrac{\partial N_i}{\partial x'} & 0 & 0 \\ 0 & \dfrac{\partial N_i}{\partial y'} & 0 \\ \dfrac{\partial N_i}{\partial y'} & \dfrac{\partial N_i}{\partial x'} & 0 \end{bmatrix}, \quad \mathbf{B}_{\mathrm{b}i}^{k} = N^{k}\,\mathbf{B}_{\mathrm{b}i}^{o} \quad i = 1, 2, 3$$

$$\bar{\mathbf{B}}_{\mathrm{b}_i}^{k} = \mathbf{B}_{\mathrm{b}_{i-3}}^{k}\mathbf{e}_{i-3}, \qquad i = 4, 5, 6$$

$$\underset{(2\times33)}{\mathbf{B}_{\mathrm{s}}^{k}} = \mathbf{J}^{-1}\mathbf{P}\underset{(3\times12)}{\left[\mathbf{B}_{\mathrm{s}}^{k},\right.} \quad \underset{(3\times12)}{\mathbf{B}_{\mathrm{s}}^{k+1},} \quad \underset{(3\times9)}{\left.\mathbf{B}_{\mathrm{w}}\right]}$$

$$\mathbf{B}_{\mathrm{s}}^{k} = \left[\begin{array}{ccc:ccc:ccc:ccc} a_{12} & b_{12} & 0 & a_{12} & b_{12} & 0 & 0 & 0 & 0 & c_{12} & 0 & 0 \\ 0 & 0 & 0 & \dfrac{a_{23}}{\sqrt{2}} & \dfrac{b_{23}}{\sqrt{2}} & 0 & \dfrac{a_{23}}{\sqrt{2}} & \dfrac{b_{23}}{\sqrt{2}} & 0 & 0 & \dfrac{c_{23}}{\sqrt{2}} & 0 \\ a_{13} & b_{13} & 0 & 0 & 0 & 0 & a_{32} & b_{32} & 0 & 0 & 0 & c_{32} \end{array}\right]$$

$$\mathbf{B}_{\mathrm{s}}^{k+1} = -\mathbf{B}_{\mathrm{s}}^{k}$$

$$\mathbf{B}_{\mathrm{w}} = \begin{bmatrix} 0 & 0 & -1 & 0 & 0 & 1 & 0 & 0 & 0 \\ 0 & 0 & 0 & 0 & 0 & -\dfrac{1}{\sqrt{2}} & 0 & 0 & \dfrac{1}{\sqrt{2}} \\ 0 & 0 & -1 & 0 & 0 & 0 & 0 & 0 & 1 \end{bmatrix}$$

$$\mathbf{P} = \begin{bmatrix} 1-\eta & -\sqrt{2}\eta & \eta \\ \xi & \sqrt{2}\xi & 1-\xi \end{bmatrix}$$

$$a_{ij} = -\frac{c_i\, l^{ij}}{2h^{k}}; \quad b_{ij} = -\frac{s_i\, l^{ij}}{2h^{k}}; \quad c_{ij} = -\frac{2l^{ij}}{3h^{k}}$$

c_i, s_i = components of vector $\mathbf{e}_i = [c_i, s_i]^{\mathrm{T}}$, i = 1,2,3

l^{ij} = length of the side ij

h^{k} = thickness of kth layer

$\mathbf{J}$ = jacobian matrix

Appendix E

E.0.1. Local stiffness matrix for one single layer of the laminated shell triangle

$$\mathbf{K}^{\prime(e)} = \mathbf{K}_{\mathrm{b}}^{\prime(e)} + \mathbf{K}_{\mathrm{s}}^{\prime(e)}$$

$$\mathbf{K}_{\mathrm{b}}^{\prime(e)} = \frac{h^{k}}{6}\begin{bmatrix} 2\mathbf{K}_{\mathrm{bb}}^{\prime} & \mathbf{K}_{\mathrm{bb}}^{\prime} & \mathbf{0} \\ \mathbf{K}_{\mathrm{bb}}^{\prime} & 2\mathbf{K}_{\mathrm{bb}}^{\prime} & \mathbf{0} \\ \mathbf{0} & \mathbf{0} & 6\mathbf{K}_{\mathrm{oo}}^{\prime} \end{bmatrix}$$

where

$$\underset{(12\times12)}{\mathbf{K}_{\mathrm{bb}}^{\prime}} = \int_{A^{(e)}}\left[\hat{\mathbf{B}}_{\mathrm{b}}^{k}\right]^{\mathrm{T}}\mathbf{D}\hat{\mathbf{B}}_{\mathrm{b}}^{k}\,\mathrm{d}A$$

with

$$\hat{\mathbf{B}}_{\mathrm{b}}^{k} = \left[\mathbf{B}_{\mathrm{b}}^{o}, \mathbf{B}_{t}^{k}\right]$$

$$\mathbf{B}_{t}^{k} = \left[\bar{\mathbf{B}}_{\mathrm{b}4}^{k}, \bar{\mathbf{B}}_{\mathrm{b}5}^{k}, \bar{\mathbf{B}}_{\mathrm{b}6}^{k}\right]$$

and

$$\underset{(9\times9)}{\mathbf{K}_{\mathrm{oo}}^{\prime}} = \int_{A^{(e)}}\mathbf{B}_{\mathrm{b}}^{o\,\mathrm{T}}\mathbf{D}\mathbf{B}_{\mathrm{b}}^{o}\,\mathrm{d}A$$

$$\mathbf{K}_{\mathrm{s}}^{\prime(e)} = h^{k}\int_{A^{(e)}}\left[\mathbf{B}_{\mathrm{s}}^{k}\right]^{\mathrm{T}}\mathbf{D}\mathbf{B}_{\mathrm{s}}^{k}\,\mathrm{d}A$$

References

[1] Reddy JN. A refined nonlinear theory of plates with transverse shear deformation. Int J Solids Struct 1987;20:881–96.

[2] Reddy JN. A generalization of two-dimensional theories of laminated composite plates. Commun Appl Numer Meth 1987;3:113–80.

[3] Reddy JN. On refined computational models of composite laminates. Int J Numer Meth Engng 1989;27:361–82.

[4] Zienkiewicz OC, Taylor RL, Papadopoulus P, Oñate E. Plate bending elements with discrete constraints: New triangular element. Comput Struct 1990;35:505–22.

[5] Papadopoulus P, Taylor RL. A triangular element based on Reissner–Mindlin plate theory. Int J Num Meth Engng 1990;30:1029–49.

[6] Oñate E, Taylor RL, Zienkiewicz OC. Consistent formulation of shear constrained Reissner–Mindlin plate elements. In: Kuhn G., Mang H., editors. Discretization Methods in Structural Mechanics. Berlin: Springer, 1990.

[7] Oñate E, Zienkiewicz OC, Suárez B, Taylor RL. A methodology for deriving shear-constrained Reissner–Mindlin plate elements. Int J Numer Meth Engng 1992;33:345–67.

[8] Oñate E, Castro J. Derivation of plate elements based on assumed shear strain fields. In: Ladeveze P, Zienkiewicz OC. editors. New Advances in Computational Structural Mechanics. Oxford: Elsevier, 1992.

[9] Zienkiewicz OC, Taylor RL. The Finite Element Method, 4th Ed., McGraw Hill, vol. I (1989), vol. II (1990).

[10] Oñate E, Botello S, Miquel J. A triangular element for analysis of composite laminated plates using a substructuring technique. In: International Meeting on de Cinquante ans de Recherche en Acoustique et Mecanique, Laborative de Mecanique et Acoustique, CNRS, Marseille, 1991. p. 8–10 April.

[11] Miquel J, Botello S, Oñate E. A finite element formulation for analysis of composite laminated shells. Journal of Iberoamerican Applied Research 1992;21:235–47.

[12] Botello S. Análisis de estructuras multilaminares por el método de los elementos finitos. Ph.D. Thesis. Univ. Politécnica de Catalunya, Barcelona (in Spanish), 1993.

[13] Owen DRJ, Li ZH. A refined analysis of laminated plates by finite element displacement methods-I. Fundamentals and static analysis; II Vibration and stability. Comp and Struct 1987;26:907–23.

[14] Owen DRL, Li ZH. Elasto-plastic numerical analysis of anisotropic laminated plates by a refined finite element model. In: Owen R, Hinton E, Oñate E, editors. Computational Plasticity: Models Software and Applications. Swansea: Pineridge Press, 1987. p. 749–75.

[15] Owen DRJ, Li ZH. Elasto-plastic numerical analysis of anisotropic laminated plates by a refined finite element model. Comput Meth Appl Mech Engng 1988;70:349–65.

[16] Oñate E, Oller S, Botello S, Miquel J. 1991. Análisis de estructuras de materiales compuestos. Monografía CIMNE 11. (in Spanish) .

[17] Noor AK. Free vibrations of multilayered composite plates. AIAA 1975;11:1038–30.

[18] Stavsky Y. Bending and stretching of laminated plates. ASCE J Engng Mech 1961;87:31–56.

[19] Barbat A, Miquel J. 1994. Estructuras sometidas a acciones sísmicas. CIMNE, Barcelona (in Spanish).

[20] Oñate E. 1995. Análisis de Estructuras por el Método de los Elementos Finitos. CIMNE, Barcelona (in Spanish).